Available online at www.sciencedirect.com
ScienceDirect
J. of Supercritical Fluids 42 (2007) 157–163
THE JOURNAL OF Supercritical Fluids
www.elsevier.com/locate/supflu

Characterization of oxide films grown on 316L stainless steel exposed to H_2O_2-containing supercritical water

Xin Gao *, Xinqiang Wu, Zhaoen Zhang, Hui Guan, En-hou Han

Environmental Corrosion Center, Institute of Metal Research, Chinese Academy of Sciences, 62 Wencui Road, Shenyang 110016, PR China

Received 4 July 2006; received in revised form 19 December 2006; accepted 30 December 2006

Abstract

The characterization of microstructure and chemical compositions of oxide films formed on surfaces of stainless steels is necessary for understanding of corrosion processes and environmentally assisted cracking. In this study, the morphologies, microstructure and chemical compositions of oxide films grown on 316L stainless steel exposed to H_2O_2-containing supercritical water (SCW) were investigated using a scanning electron microscope equipped with an energy-dispersive X-ray spectrometer (EDX), an X-ray photoelectron spectroscopy (XPS) analyzer and an X-ray diffraction (XRD) analyzer. A duplex-layer structure was identified in the oxide films. The loose outer layer was rich in Fe, while the compact inner layer was rich in Cr and Fe. In addition, Ni enrichment was observed at the interface between the metal matrix and oxides. The surface oxides tended to change with an increase in water temperature. The possible growth mechanism of the oxide films on 316L stainless steel in SCW environments is believed to be similar to that in high-temperature water, namely metal dissolution/oxide precipitation mechanism and solid-state growth mechanism.

Keywords: Supercritical water oxidation; Stainless steel; Characterization; Oxide film

1. Introduction

At temperatures above 374.15 °C and pressures above 22.1 MPa, water is in a supercritical state whose properties change significantly compared with ambient water. Organics, such as hydrocarbons, and gases like oxygen, become completely miscible with supercritical water (SCW). Due to the outstanding physical and chemical properties of SCW, a new technology – supercritical water oxidation (SCWO) which can effectively and safely dispose various organic wastes [1–4] – has been developed. SCWO has the advantage of the single-phase behavior of the reaction environment, high conversion efficiencies (as high as 99.99% and more) and few undesirable by-products [5]. Therefore, SCWO has been used for disposal of toxic and hazardous wastes. However, severe reactor corrosion occurs in SCWO processes since reactors capable of accommodating elevated temperatures and pressures must be used and, potentially, very aggressive environments are present when anions like chlorides or sulfates exist [6].

In previous papers [7–9], problems dealing with SCWO processes have been discussed in detail. Under high-temperature and supercritical water environment, there are three main problems: severe reactor corrosion occurring in the process of SCWO, such as pitting corrosion, general corrosion, intergranular corrosion and stress corrosion cracking [8]; serious plugging of the reactors caused by precipitating salts at supercritical temperatures and low densities [7]; hard to perform cost evaluations, especially for the scale-up of SCWO plants to an industrial scale, due to the lack of experimental data [7].

Corrosion in aqueous systems up to the supercritical temperature is determined by several parameters, such as the physical properties of water, the dissociation of attacking acids or salts, and the solubility of gases, oxides, and corrosion products in the solvent [10]. Among these parameters, corrosion products, especially oxide films, are worth further studying because the chemical compositions and structure of the films are important for understanding of corrosion process and possible environmentally assisted cracking (EAC).

Most of the previous studies [11–16] have focused on the characterization of oxide films formed on stainless steels in high-temperature and high-pressure water (temperature < 350 °C and pressure < 20 MPa). It was found that the oxide films mainly

* Corresponding author. Tel.: +86 24 2399 0892; fax: +86 24 2389 4149.
E-mail addresses: xgao@imr.ac.cn, gaoxin0101@163.com (X. Gao).

0896-8446/$ – see front matter © 2007 Elsevier B.V. All rights reserved.
doi:10.1016/j.supflu.2006.12.020

consisted of double layers [11–14]: an outer oxide layer with a large particle and an intermediate or small particle (hematite [α-Fe_2O_3] structure) and a very fine-grain inner layer with a chromium-enriched Fe_3O_4-type structure [11]. The outer layer is thicker than the inner layer; while the inner layer is more compact than the outer layer. Many efforts have been given to the study of the relationship between the oxide films and initiation of EAC. Through experiments, Wang et al. indicated that oxidation plays a primary role, at least at the very initial stage of EAC in simulated boiling water reactor high-temperature water. The metal oxidation process is influenced by the microstructural defects in materials such as grain boundaries, etc. [17].

The oxide films depend on the corrosive circumstances. The oxide film formed under H_2O_2 environments consists mainly of α-Fe_2O_3, while that under O_2 environments consists of Fe_3O_4 [18,19]. Furthermore, oxidation at the very surface of the film is much more enhanced under an H_2O_2 environment than that under an O_2 environment. For the specimens exposed to H_2O_2, a drop in Cr concentration in the oxide film was confirmed, which resulted in less corrosion resistance to general corrosion of stainless steel in coolants containing H_2O_2 [19].

Compared to studies on stainless steels in high-temperature and high-pressure water, little work has focused on oxide films formed in SCW due to the difficulty of experimental techniques. Undoubtedly, oxide films are also very important to understand the corrosion process and EAC in SCW environments. In the present work, oxide films grown on the surface of 316L stainless steel (SS) exposed to H_2O_2-containing SCW were investigated in detail with a scanning electron microscope (SEM) equipped with an energy-dispersive X-ray spectrometer (EDX), an X-ray photoelectron spectroscopy (XPS) analyzer and an X-ray diffraction (XRD) analyzer. The morphologies, microstructure and chemical compositions of the oxide films were examined. The possible growth mechanism of the oxide films in SCW environments is also discussed.

2. Experimental

The material used in the present study was solution-treated 316L stainless steel sheet that had a chemical composition as given in Table 1. Rectangular specimens (20 mm × 12.5 mm) were cut from the steel sheet of 2.5 mm thickness. The specimens were polished with emery paper down to #1000 grit and finally mechanically finished to a 1.5 μm diamond finish. Prior to each experiment, the specimens were cleaned with acetone and ultrasonically rinsed with deionized water for 5 min.

The experiments were performed with an autoclave and a continuous flowing SCWO system. Fig. 1 shows a schematic representation of the supercritical corrosion system configuration used, which consisted of an alloy 625 autoclave, a high-pressure liquid chromatogram (HPLC, Eldex Inc. BBB-4-2) pump, a preheater, a heat exchanger, a back pressure regulator (BPR), thermocouples, a pressure sensor and a computer. The autoclave, with an inner diameter of 60 mm, a wall thickness of 45 mm and a length of 270 mm had a capacity of 850 ml solution. The system temperature was monitored by two thermocouples placed into the forepart of the preheater and the top of the solution in the autoclave, respectively. The pressure sensor was equipped in the system to check the pressure simultaneously. The system pressure was provided by the HPLC pump and controlled by the BPR. The computer was used to control the temperature and pressure.

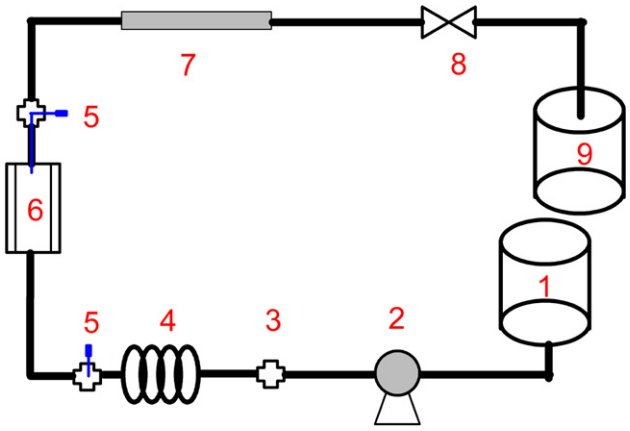

Fig. 1. Schematic diagram of SCWO test system. (1) Feed solution; (2) HPLC pump; (3) pressure sensor and rupture disc; (4) preheater; (5) thermocouples; (6) autoclave; (7) heat exchanger; (8) back pressure regulator (9) effluent.

Table 1
Chemical compositions of type 316L stainless steels used (wt%)

C	Si	Cr	Ni	Mo	P	Fe
0.03	0.56	17.00	10.18	2.68	<0.045	Bal.

During the tests, the specimens were mounted on a rack and put into the autoclave. The surface of the rack was spattered with zirconia to avoid contacting the autoclave. The pump provided 2.0% H_2O_2 at the flow rate of 2.5 ml/min. The feed solution was preheated and then entered the autoclave. In the autoclave, the solution was heated to the experimental temperature (400, 450 and 500 °C). The effluent was cooled to room temperature by the heat exchanger and then drained out of the system. The pressure maintained at 24 MPa. Duration of the experiments was 100 h.

After the experiments, the specimens were cleaned and dried. The surface morphologies of oxide films on the specimens were examined using XL30 SEM. The chemical compositions of the oxide films were analyzed by XPS (PHI-5300 ESCA), XRD (X'Pert PRO PANalytical) and EDX.

To investigate the cross sections of the oxide films, some tested specimens were activated in an activated solution at 70 °C for 1 min. Then they were coated in electroless Ni–P plating solution at 50 °C for 10 min to protect the oxide films. The activated solution was as: $PdCl_2$ 2 g/L; HCl 200 ml/L; $SnCl_2$ 4 g/L. The plating solution was: $NiSO_4{\cdot}6H_2O$ 20 g/L; $NaH_2PO_2{\cdot}H_2O$ 30 g/L; $Na_3C_6H_5O_7{\cdot}H_2O$ 10 g/L [14]; NH_4Cl 30 g/L; pH 9–10. The coated specimens were mounted with epoxy resin and then polished. The corresponding cross sections of the oxide films were examined using SEM and EDX.

3. Results

3.1. Morphologies of the oxide films

Fig. 2 shows SEM images of surfaces of 316L SS after 100 h test in SCW at different temperatures. At 400 °C, the oxide film was relatively compact and mainly composed of large lath-like grains. Different from the film formed at 400 °C, the film formed at 450 °C consisted of cystiform grains with different sizes. Some small pores were observed among the grains. The oxide film formed at 500 °C looked desultory with many big pores among the grains.

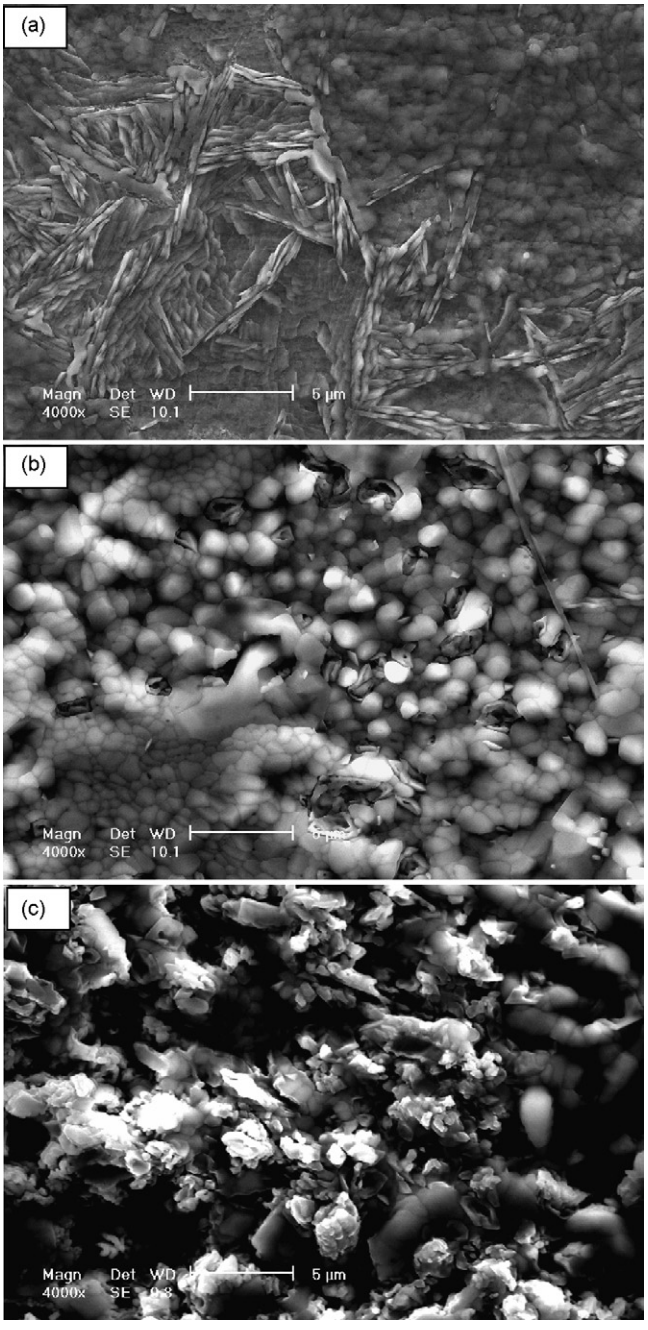

Fig. 2. Surface morphologies of oxide films formed on 316L SS at: (a) 400 °C (b) 450 °C (c) 500 °C.

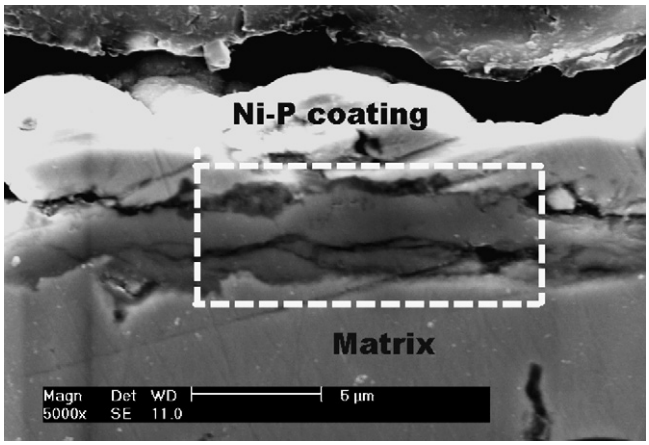

Fig. 3. Cross section of a continuous oxide film formed at 500 °C.

Figs. 3 and 4 show the morphologies of cross sections of the oxide films. Fig. 3 is an image of a continuous film. A double-layer structure was observed except for the outmost Ni–P coating. There was a micro-crack between the outer layer and the inner layer. The maximum thickness of the outer oxide film was about 2.2 μm and that of the inner film was about 1.4 μm. The thickness of the above two layers was much thinner than that of ferritic-martensitic alloy NF616 exposed to supercritical water [20] as for the latter, the thickness of the outer layer was about 7.2 μm and that of the inner layer was about 5.4 μm. Fig. 4 is an image of an oxide mound. There was also a micro-crack between the outer layer and the inner layer. The maximum thickness of the outer layer was about three times that of the inner layer. Some cavities were observed between the two layers because some oxides had spalled off during the polishing. The separation, to some extent, indicated a relatively weak bonding force between the outer layer and the inner layer. No obvious crack was found between the inner layer and the matrix, perhaps indicating a relatively good bonding force between them.

3.2. Composition of the oxide films

Figs. 5–8 show the EDX results of the oxide films formed in 500 °C supercritical water. The outer layer was rich in Fe,

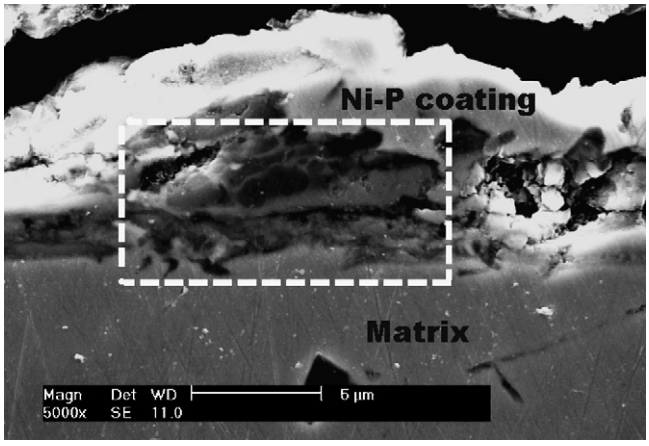

Fig. 4. Cross section of an oxide mound formed at 500 °C.

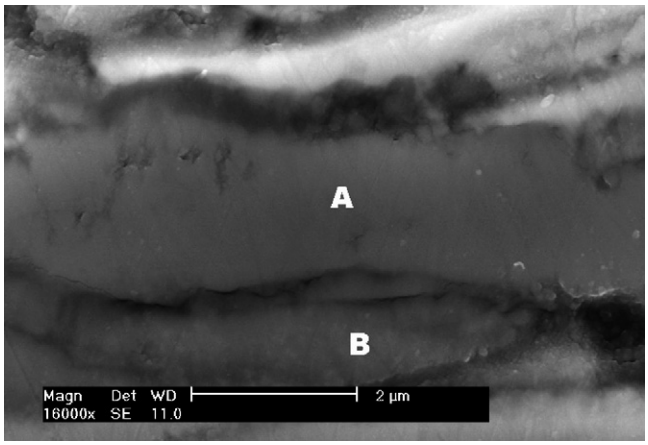

Fig. 5. Cross section of a continuous oxide film formed at 500 °C (enlargement of marked zone in Fig. 3).

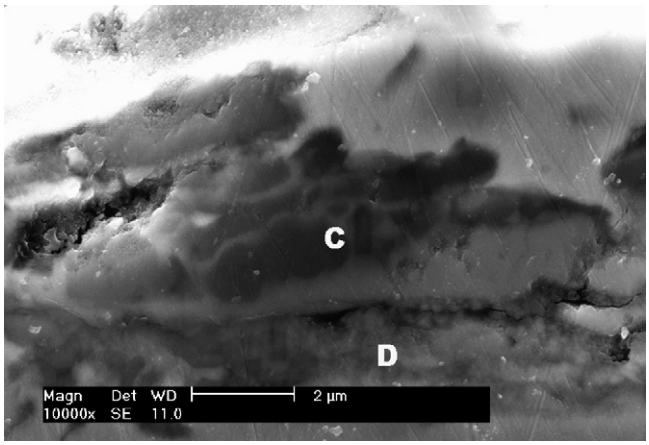

Fig. 7. Cross section of an oxide mound formed at 500 °C (enlargement of marked zone in Fig. 4).

while the inner layer was rich in Cr and Fe, which agreed well with previous studies on oxide films formed in high-temperature water [12,16]. Kim found that the oxide film formed on type 316 stainless steel in 288 °C water containing 200 ppb H_2O_2 mainly consisted of two oxide layers: an outer layer of γ-Fe_2O_3 and an inner layer of Fe-enriched and Cr-enriched oxides [12]. Terachi et al. indicated that the oxide film formed on 316 stainless steel exposed to simulated pressurized water reactor primary water at 320 °C had a double-layer structure: the outer layer was composed mainly of iron oxide and relatively chromium-rich oxide was recognized in the inner layer [16].

The line scan analysis results are shown in Figs. 9 and 10. The outer layer of the oxide film consisted mainly of Fe oxide. In the inner layer, the content of Cr oxide increased sharply and that of Fe oxide decreased. In addition, Ni enrichment was observed at the interface between the metal matrix and inner layer.

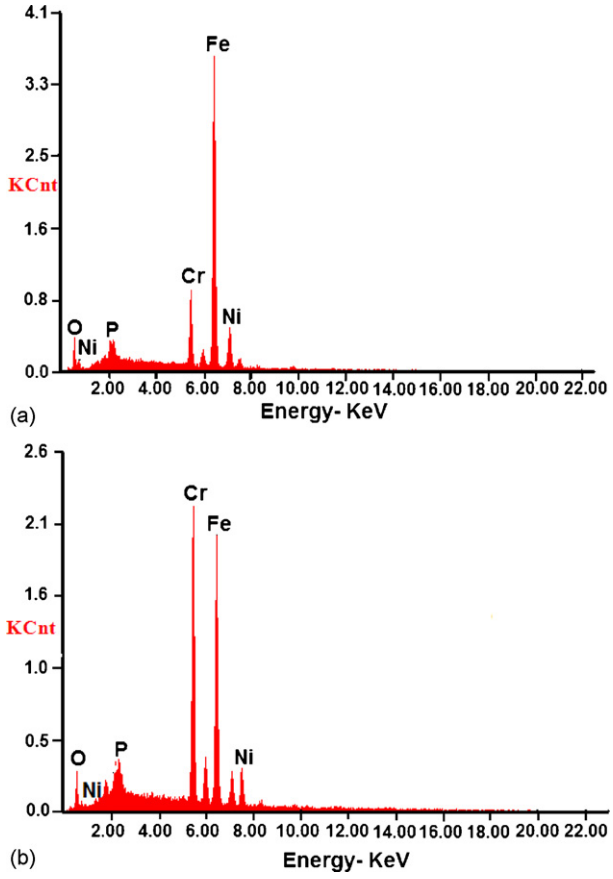

Fig. 6. EDX spectra of oxide films, (a): outer layer (corresponding to A zone shown in Fig. 5); (b): inner layer (corresponding to B zone shown in Fig. 5).

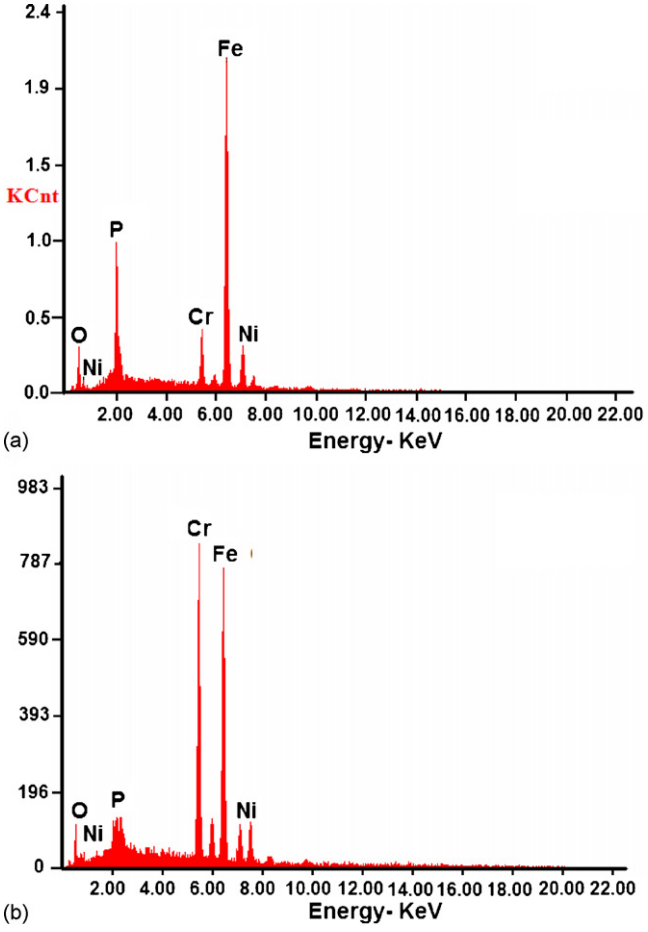

Fig. 8. EDX spectra of oxide films, (a): outer layer (corresponding to C zone shown in Fig. 7); (b): inner layer (corresponding to D zone shown in Fig. 7).

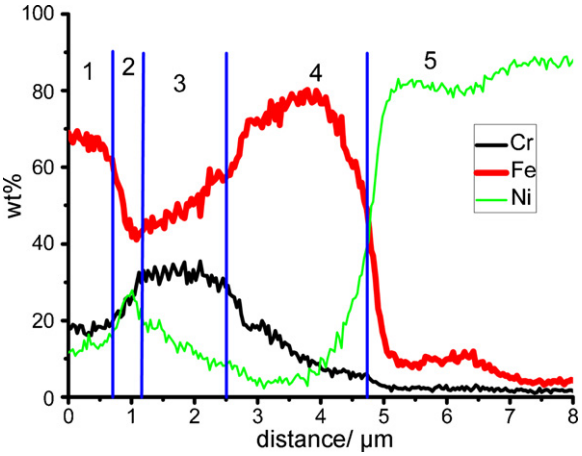

Fig. 9. EDX line scan profiles of oxide films for analysis area shown in Fig. 10.

Fig. 11 shows typical XPS spectra of the specimens tested in SCW. At 400 °C, the binding energy (BE) of O 1s was 530.1 eV, corresponding to the form of O^{2-} in oxide [21]; the BE of Cr 2p3/2 core-level peak was centred at 577.52 eV and the BE of Cr 2p1/2 was centred at 587.30 eV, corresponding to Cr^{3+} in $Cr(OH)_3$ [22,23]; the BE of Fe 2p3/2 was 712.86 eV, corresponding to Fe^{3+} in α-FeOOH [24]. Also the lath-like appearance of surface oxides (Fig. 2a), to some extent, indicated the existence of goethite α-FeOOH in the oxide film formed in SCW at 400 °C. At 450 °C, the BE of O 1s was 530.9 eV, corresponding to the form of O^{2-} in oxide [21]; the BE of Cr 2p3/2 was 578.05 eV and that of Cr 2p1/2 was 586.88 eV, corresponding to Cr_2O_3 [22,25] and $Cr(OH)_3$ [23]; the BE of Fe 2p3/2 was 712.09 eV, corresponding to α-FeOOH [24]. At 500 °C, the BE of O 1s was 531.4 eV, corresponding to the form of O^{2-} in oxide [21]; the BE of Cr 2p3/2 was 576.89 eV and that of Cr 2p1/2 was 586.19 eV, corresponding to Cr_2O_3 [26,27]; the BE of Fe 2p3/2 was 711.79 eV, corresponding to α-FeOOH and γ-FeOOH [24].

Fig. 12 shows the XRD profile from 316L SS tested in SCW at 500 °C for 100 h. The peaks corresponding to Cr_2O_3 and FeOOH were observed, in accordance with the previous XPS results, but the existence of Cr_2O_5 was different from the XPS results.

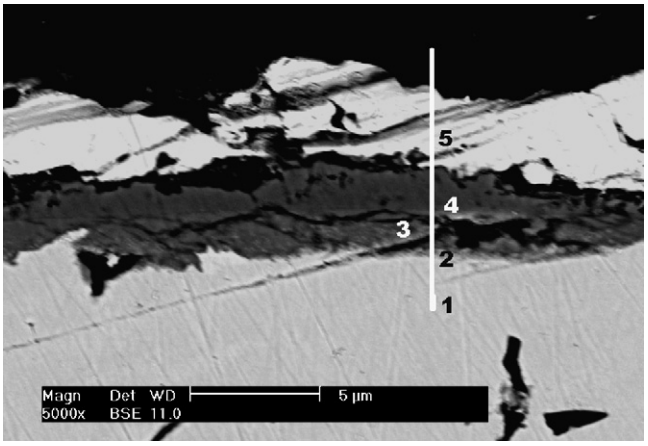

Fig. 10. Back scattering cross section of oxide films formed at 500 °C, 1: matrix; 2: matrix/inner layer interface; 3: inner layer; 4: outer layer; 5: Ni–P coating.

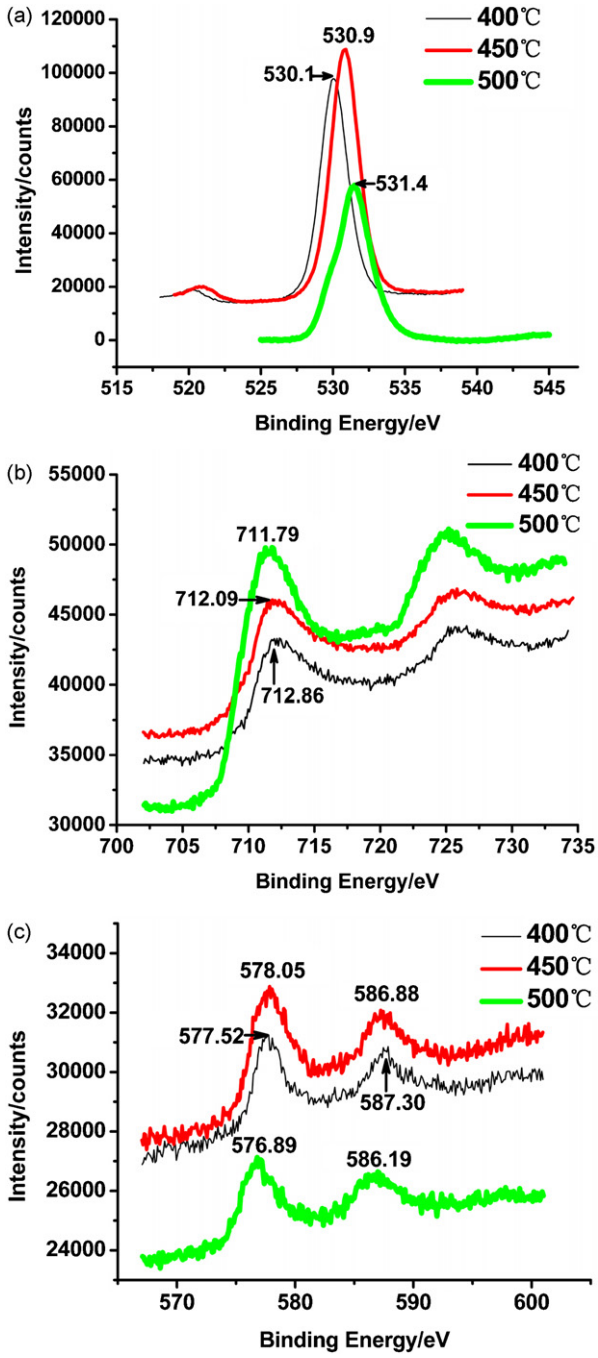

Fig. 11. XPS spectra of 316L stainless steels after contacted with SCW at 400, 450 and 500 °C for 100 h: (a) O (b) Fe (c) Cr.

4. Discussion

Previously, much work has focused on the mechanism of oxide films grown on the stainless steels in high-temperature water [28,29]. Several typical mechanisms, such as solid-state growth mechanism and metal dissolution/oxide precipitation mechanism, have been proposed and generally accepted [28]. In general, the outer layer grows via a metal dissolution and oxide precipitation mechanism and the inner layer grows via a solid-state growth mechanism. In the present work, a double-layer oxide film formed in SCW was observed. It is believed that the

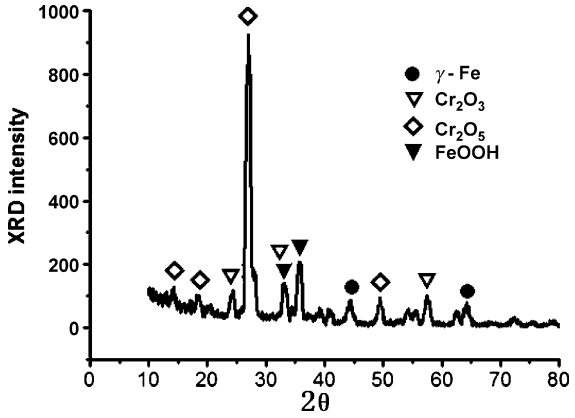

Fig. 12. XRD profile of 316L stainless steel after contacted with SCW at 500 °C for 100 h.

growth mechanism of oxide films on 316L stainless steel in SCW is similar to that in high-temperature water, namely metal dissolution/oxide precipitation mechanism and solid-state growth mechanism. In high-temperature water, H_2O_2 may decompose into OH^- as follows:

$$H_2O_2 + (M) \rightarrow 2OH^- + (M) \quad (1)$$

where the collision partner, M, is water [30]. Metal ions containing Fe, Cr and Ni can dissolve at the active sites at the base of pores [28]. With an increase in dissolved metal concentrations, the metal cations may combine with anions to form oxides or hydroxides and precipitate on the surface of the specimen. Because the diffusion velocity of Fe is faster than that of Cr and Ni and Fe oxide has a high negative free energy, Fe oxides precipitate first and form the outer layer. Cr diffuses more slowly than Fe, so they are retained and enriched in the inner layer. The outer layer grows by iron dissolving in water in the pores and then precipitates out at the outer oxide surface. The fine-grained inner layer grows by access of water through oxide micropores, grain boundaries and other circuit paths in the oxides [31,28].

In the present work, Ni enrichment was observed at the interface between the matrix and inner layer (Fig. 9). This may be due to its slower rate of oxidation compared to Cr and Fe.

The XPS results show that with an increase in temperature, Cr oxides in oxide films tended to change from $Cr(OH)_3$ to Cr_2O_3 (Fig. 11c), indicating a dehydrogenation process with increasing temperature. Fe oxides changed from α-FeOOH to mixed α-FeOOH and γ-FeOOH (Fig. 11b). Compared to γ-FeOOH, α-FeOOH is more thermodynamically stable. Moreover, the layer consisting of α-FeOOH is compact while the one consisting of γ-FeOOH is loose [32]. This may explain the previous SEM results that the film formed at 400 °C appeared relatively compact, while the film formed at 500 °C looked desultory (Fig. 2). In addition, increasing temperature increases the numbers of defects in an oxide film [33]. As a result, the oxide films probably became less protective with an increase in temperature.

Hydroxides have been detected in the outer layer on Fe and stainless steels in supercritical water by Raman spectroscopy [34] and also by XPS in simulated boiling water reactor coolant [35]. In the present work, both XPS and XRD showed that Fe existed in the oxide films in the form of FeOOH (Figs. 11b and 12), in accordance with the previous results.

Cr_2O_5 was detected by XRD (Fig. 12), which was different from the XPS results (Fig. 11b). The reasons for the above difference remain still unknown and need to be clarified by further work.

According to the present results, the oxide films formed on 316L SS exposed to H_2O_2-containing supercritical water showed poor protection against corrosion. This seemed to suggest that 316L SS is not suitable for applications in SCWO environments.

5. Conclusion

The oxide films grown on 316L stainless steel exposed to H_2O_2-containing supercritical water were investigated using a scanning electron microscope equipped with an energy-dispersive X-ray spectrometer, an X-ray photoelectron spectroscopy analyzer and an X-ray diffraction analyzer. Conclusions could be drawn as follows.

The oxide films were found to become less continuous with an increase in temperature. The oxide films formed in SCW consisted of double layers: the loose outer layer with Fe enrichment and the compact inner layer with Cr and Fe enrichment. Ni enrichment was observed at the interface between the metal matrix and oxide film. With an increase in temperature, Cr oxides in oxide films tended to change from $Cr(OH)_3$ to Cr_2O_3, Fe oxides changed from α-FeOOH to mixed α-FeOOH and γ-FeOOH.

The growth mechanism of oxide films on 316L SS in SCW is believed to be similar to that in high-temperature water, namely metal dissolution/oxide precipitation mechanism and solid-state growth mechanism.

It was found that 316L SS experienced severe attack when exposed to H_2O_2-containing supercritical water in the present study, suggesting that 316L SS is not suitable for applications in SCWO environments.

Acknowledgements

This study was jointly supported by the Special Funds for the Major State Basic Research Projects (2006CB605000), the Science and Technology Foundation of China (50534010), the Science and Technology Foundation of Liaoning Province, and the Innovation Fund of Institute of Metal Research (IMR), Chinese Academy of Sciences (CAS).

References

[1] Y. Tsuchiya, N. Saito, K. Hiruta, Y. Akai, Corrosion behavior of metals for SCWO reactors for organic waste processing plants, in: Corrosion 2001, National Association of Corrosion Engineers, Houston, TX, 2001 (paper no. 01357).

[2] Y. Ikushima, M. Son, H. Kim, Y. Kurata, K. Hatakeda, Corrosion behavior of metals in supercritical water solutions in the presence of salts, in: Corrosion 2001, National Association of Corrosion Engineers, Houston, TX, 2001 (paper no. 01364).

[3] D.B. Mitton, Y.S. Kim, J.H. Yoon, S. Take, R.M. Latanision, Corrosion of SCWO constructional materials in Cl^- containing environments, in: Corrosion 99, National Association of Corrosion Engineers, Houston, TX, 1999 (paper no. 257).
[4] P. Kritzer, N. Boukis, E. Dinjus, Investigations of the corrosion of reactor materials during the process of supercritical water oxidation (SCWO), in: Proceeding of the Sixth Meeting on Supercritical Fluids, Nottingham, UK, 1999, pp. 433–442.
[5] M. Weber, B. Wellig, P.R.V. Rohr, SCWO apparatus design-towards industrial availability, in: Corrosion 99, National Association of Corrosion Engineers, Houston, TX, 1999 (paper no. 258).
[6] D.B. Mitton, J.H. Yoon, R.M. Latanision, An overview of corrosion phenomena in SCWO systems for hazardous waste destruction, Zairyo-to-Kankyo 49 (2000) 130–137.
[7] P. Kritzer, E. Dinjus, An assessment of supercritical water oxidation (SCWO) existing problems, possible solutions and new reactor concepts, Chem. Eng. J. 83 (2001) 207–214.
[8] P. Kritzer, Corrosion in high-temperature and supercritical water and aqueous solutions: a review, J. Supercrit. Fluids 29 (2004) 1–29.
[9] P. Kritzer, N. Boukis, E. Dinjus, Review of the corrosion of nickel-based alloys and stainless steels in strongly oxidizing pressurized high-temperature solutions at subcritical and supercritical temperatures, Corrosion 56 (2000) 1093–1104.
[10] P. Kritzer, N. Boukis, E. Dinjus, Factors controlling corrosion in high-temperature aqueous solutions: a contribution to the dissociation and solubility data influencing corrosion processes, J. Supercrit. Fluids 15 (1999) 205–227.
[11] Y.J. Kim, Characterization of the oxide film formed on type 316 stainless steel in 288 °C water in cyclic normal and hydrogen water chemistries, Corrosion 51 (1995) 849–860.
[12] Y.J. Kim, Analysis of oxide film formed on type 304 stainless steel in 288 °C water containing oxygen, hydrogen, and hydrogen peroxide, Corrosion 55 (1999) 81–88.
[13] C.S. Kumai, T.M. Devine, Oxidation of iron in 288 °C, oxygen-containing water, Corrosion 61 (2005) 201–218.
[14] S. Wang, Y. Takeda, T. Shoji, N. Kawaguchi, Observation of the oxide film formed in high temperature water by applying electroless Ni–P coating, J. Nucl. Sci. Technol. 41 (2004) 777–779.
[15] Y. Nemoto, Y. Miwa, M. Kikuchi, Y. Kaji, T. Tsukada, H. Tsuji, Development of analytical method and study about microstructure of oxide films on stainless steel, J. Nucl. Sci. Technol. 39 (2002) 996–1001.
[16] T. Terachi, K. Fujii, K. Arioka, Microstructral characterization of SCC crack tip and oxide film for SUS 316 stainless steel in simulated PWR primary water at 320 °C, J. Nucl. Sci. Technol. 42 (2005) 225–232.
[17] S. Wang, T. Shoji, N. Kawaguchi, Initiation of environmentally assisted cracking in high-temperature water, Corrosion 61 (2005) 137–144.
[18] Y. Wada, A. Watanabe, M. Tachibana, K. Ishida, N. Uetake, S. Uchida, K. Akamine, M. Sambongi, S. Suzuki, K. Ishigure, Effects of hydrogen peroxide on intergranular stress corrosion cracking of stainless steel in high temperature water. (IV) Effects of oxide film on electrochemical corrosion potential, J. Nucl. Sci. Technol. 38 (2001) 183–192.
[19] Y. Murayama, T. Satoh, S. Uchida, Y. Satoh, S. Nagata, T. Satoh, Y. Wada, M. Tachibana, Effects of hydrogen peroxide on intergranular stress corrosion cracking of stainless steel in high temperature water. (V) Characterization of oxide film on stainless steel by multilateral surface analyses, J. Nucl. Sci. Technol. 39 (2002) 1199–1206.
[20] G.S. Was, T.R. Allen, Time, temperature, and dissolved oxygen dependence of oxidation of austenitic and ferritic-martensitic alloys in supercritical water, in: Proceedings of ICAPP'05, Seoul, Korea, 2005 (paper 5690).
[21] L. Zhang, Development of supercritical water oxidation experiment systems and studies of corrosion behavior of materials under SCWO environment, Doctoral Dissertation, 2003 (in Chinese).
[22] D. Shuttleworth, Preparation of metal-polymer dispersions by plasma techniques. An ESCA investigation, J. Phys. Chem. 84 (1980) 1629–1634.
[23] E. Desimoni, C. Malitesta, P.G. Zambonin, J.C. Riviere, An X-ray photoelectron spectroscopic study of some chromium-oxygen systems, Surf. Interface Anal. 13 (1988) 173–179.
[24] Z. Zhang, Studies of corrosion behavior and mechanism of GH625 alloy and 316L stainless steel in supercritical water oxidation system, Doctoral Dissertation, 2005 (in Chinese).
[25] S. Mischler, H.J. Mathieu, D. Landolt, Investigation of a passive film on an iron-chromium alloy by AES and XPS, Surf. Interface Anal. 11 (1988) 182.
[26] G.C. Allen, M.T. Curtis, A.J. Hooper, P.M. Tucker, X-Ray photoelectron spectroscopy of chromium–oxygen systems, J. Chem. Soc., Dalton Trans. (1973) 1675–1683.
[27] G.C. Allen, S.J. Harris, J.A. Jutson, J.M. Dyke, A study of a number of mixed transition metal oxide spinels using X-ray photoelectron spectroscopy, Appl. Surf. Sci. 37 (1989) 111–134.
[28] B. Stellwag, The mechanism of oxide film formation on austenitic stainless steels in high temperature water, Corros. Sci. 40 (1998) 337–370.
[29] J. Robertson, The mechanism of high temperature aqueous corrosion of steel, Corros. Sci. 29 (1989) 1275–1291.
[30] E. Croiset, S.F. Rice, R.G. Hanush, Hydrogen peroxide decomposition in supercritical water, AlChE J. 43 (1997) 2343–2352.
[31] J. Robertson, The mechanism of high temperature aqueous corrosion of stainless steels, Corros. Sci. 32 (1991) 443–465.
[32] J. Wang, X. Guo, W. Zheng, J. Chen, J. Wu, Analysis of the corrosion rust on weathering steel and carbon steel exposed in marine atmosphere for three years, Corros. Prot. 23 (2002) 288–291 (in Chinese).
[33] P. Kritzer, N. Boukis, E. Dinjus, The corrosion of nickel-base alloy 625 in sub- and supercritical aqueous solutions of oxygen: a long time study, J. Mater. Sci. Lett. 18 (1999) 1845–1847.
[34] J.E. Maslar, W.S. Hurst, W.J. Bowers, J.H. Hendricks, In situ Raman spectroscopic investigation of stainless steel hydrothermal corrosion, Corrosion 58 (2002) 739–747.
[35] J. Wambach, A. Wokaun, A. Hiltpold, Oxidation of stainless steel under dry and aqueous conditions: oxidation behaviour and composition, Surf. Interface Anal. 34 (2002) 164–170.